THE ASTROPHYSICAL JOURNAL, 374:L9–L12, 1991 June 10

BROAD PASCHEN-ALPHA EMISSION IN TWO EXTREMELY INFRARED LUMINOUS SEYFERT 2 GALAXIES

DEAN C. HINES
McDonald Observatory and Department of Astronomy, RLM 15.308, University of Texas, Austin, TX 78712
Received 1991 March 8; accepted 1991 March 27

ABSTRACT

I present observations of the Paα emission line in the extremely luminous, *IRAS*-selected galaxies IRAS 20460+1925 and IRAS 23060+0505. These objects have previously been classified as Seyfert 2 galaxies based on their optical emission-line spectra, but their luminosities (greater than $10^{12}\ L_\odot$) are characteristic of QSOs. The widths of Hα are 2500 and 550 km s^{-1} (FWHM) for IRAS 20460+1925 and IRAS 23060+0505, respectively. The Paα observations reveal the presence of broad lines of width 2940 ($\pm$160) and 2900 ($\pm$270) km s^{-1} (FWHM, both corrected for the instrumental broadening). Using the narrow line strengths derived from the reddened optical line spectra, the narrow Paα line contributions to the observed Paα emission profiles have been removed. The resulting broad-line widths are $\sim$3860 and $\sim$4780 km s^{-1} for IRAS 20460+1925 and IRAS 23060+0505, respectively. The Paα measurements place constraints on the visual extinction to the BLR, $A_v > 3.6$ for IRAS 20460+1925 and $A_v \gtrsim 4.4$ for IRAS 23060+0505. Considering their bolometric luminosities and the presence of broad emission lines, I suggest that IRAS 20460+1925 and IRAS 23060+0505 should be reclassified as QSOs.

Subject headings: galaxies: nuclei — galaxies: Seyfert — infrared: spectra — quasars

1. INTRODUCTION

Frogel et al. (1989) identify IRAS 20460+1925 with a red unresolved object on the Palomar Observatory Sky Survey (POSS) prints. The object was selected as part of a survey of infrared sources with $F_\nu(60\ \mu m)/F_\nu(100\ \mu m) \geq 1.0$, $0.25 \leq F_\nu(25\ \mu m)/F_\nu(60\ \mu m) \leq 1.0$ and galactic latitude $|b| > 10°$. The galaxy IRAS 20460+1925 has an extremely flat infrared energy distribution ($\alpha_{12-100\ \mu m} \approx 0.6$, $F_\nu \propto \nu^{-\alpha}$), but the 0.5–3.5 μm energy distribution is steep, $\alpha \approx 2$–2.5 (Frogel et al. 1989). Its observed bolometric luminosity of $7 \times 10^{12}\ L_\odot$ ($z = 0.181$, $H_0 = 75$ km s^{-1} Mpc^{-1}, $q_0 = 0$), is comparable with QSO luminosities. Frogel et al. (1989) classify IRAS 20460+1925 as a Seyfert 2 (Sy 2) galaxy, although the forbidden and permitted emission lines are quite broad with full widths at half-maximum intensity (FWHM) in the range 1700–2500 km s^{-1}). The Balmer line intensity ratios imply $A_v \approx 2.2$. There is evidence for a possible weak broad component to Hα, and Frogel et al. (1989) suggest that IRAS 20460+1925 contains an obscured QSO nucleus that powers the thermal reradiation by dust. In fact, Kay & Miller (1989) find broad Hβ emission (FWHM$_b \sim 6000$ km s^{-1}) in the polarized flux spectrum.

Hill, Wynn-Williams, & Becklin (1987, hereafter HWB) report the identification of IRAS 23060+0505 with a red unresolved object on the POSS prints, as part of a program to study *IRAS* point sources having very warm infrared energy distributions [$F_\nu(25\ \mu m)/F_\nu(60\ \mu m) > 0.3$]. HWB report unusually red *JHKL'* colors and a relatively flat infrared energy distribution ($\alpha_{12-100\ \mu m} \approx 0.6$). The optical spectrum resembles a Sy 2 galaxy with narrow emission lines of width $\approx$550 km s^{-1}, but there are signs of a very weak broad wing on the long-wavelength side of Hα. HWB derive a redshift $z = 0.1738 \pm 0.0005$, and a bolometric luminosity of $3.3 \times 10^{12}\ L_\odot$. The optical continuum is very steep ($\alpha = 2.8$) and the Hα/Hβ intensity ratio implies $A_v = 3.4 \pm 0.5$.[1] Although the optical spectrum is that of a Sy 2 galaxy, the bolometric luminosity and infrared energy distribution are more typical of QSOs. HWB suggest that IRAS 23060+0505 may contain a highly obscured QSO nucleus, and that its presence might be revealed by IR spectroscopy.

Hough et al. (1991) have obtained optical and infrared polarimetry of IRAS 23060+0505, and find high, non–time-variable linear polarization rising from 1.5% in *U*-band to 7.5% in *I*-band and decreasing to 5.7% in *K*-band.[2] The polarization position angle is essentially wavelength-independent. The degree of polarization is aperture-dependent, but the polarized flux is aperture-independent, implying that the polarized light is produced within 4″ of the nucleus. Based on their polarization modeling, Hough et al. (1991) suggest that scattering of hidden QSO emission is the most likely explanation for the very unusual polarization properties. Selective extinction of emission from an obscured QSO by aligned dust grains is also a possible explanation, but the high degree of polarization would imply unusually high grain alignments compared with the dust in our Galaxy.

To investigate the possibility that IRAS 20460+1925 and IRAS 23060+0505 contain QSO nuclei obscured by dust, I have obtained *K*-band infrared spectrophotometry to look for broad Paα emission.

2. OBSERVATIONS

The observations were obtained at the f/18 focus of the McDonald 2.7 m telescope, using an infrared, cooled-grating spectrometer with a 32 channel Cincinnati Electronics InSb array detector. The instrument uses a 3″.8 × 3″.8 aperture that is configured so that all the energy of a monochromatic emission line, centered in the aperture and centered in wavelength, falls on a single pixel. To remove dark current, thermal emis-

[1] This value was misprinted as $A_v = 4.3$ in HWB (Hill 1991, private communication).

[2] Hough et al. (1991) also discuss the classification of IRAS 23060+0505 as a Sy 2 based on their spectrophotometry, and note that if Hβ is corrected for absorption assuming a normal spiral galaxy star population near the nucleus, then $A_v \sim 2.8$ for the NLR.

sion from the sky and telescope, and the fixed pattern signal of the detector, the telescope was pointed 20″ north for a 60 s sky integration for every 60 s of object integration (object-sky-sky-object). The details of the instrument and its operation are given in Lester, Harvey, & Carr (1988) (see also Lester et al. 1990).

The galaxies IRAS 20460+1925 and IRAS 23060+0505 were observed on UT 1990 September 2–3 and September 25–26. The seeing was typically 2″, but was ~1″ on UT 1990 September 26. Conditions were photometric on 1990 September 26, so all the calibrated amplitudes for the scans were scaled to those of September 26 (an adjustment of less than 10% for all scans). The total integration times were 4800 s for IRAS 20460+1925 and 6840 s for 23060+1925. The absolute wavelength scale was determined by observing an argon calibration lamp, and is accurate to better than 0.0027 μm (i.e., 0.25 pix). Atmospheric absorption features were removed by dividing the object spectrum by that of a nearby hot star (BS 7981 for IRAS 20460+1925 and BS 8826 for IRAS 23060+0505) observed before and after each long integration. Absorption from Brγ in the division star was removed by interpolating across the unresolved feature before division. For both IRAS 20460+1925 and IRAS 23060+0505 the Paα emission is well centered in the K-band, so the line profile is not affected by atmospheric absorption features. The absolute flux scale was determined by observations of infrared standard stars at similar air masses (BS 8781 for IRAS 20460+1925 and BS 0015 for IRAS 23060+0505). The flux calibration is internally consistent to 15%–20% (rms), and a comparison with the infrared photometry of HWB and Frogel et al. (1989) shows that the flux measurements agree to within 10%.

A low-resolution grating was used to maximize signal-to-noise, but to improve resolution the objects were observed at two grating tilts that shifted the spectra by ~0.5 pixel to approximate Nyquist sampling of the spectrum. I take the effective spectral resolution to be equal to the array pixel size, 0.01066 μm. The unblended argon emission line at $\lambda = 2.3140$ μm, sampled as for the observations of IRAS 23060+0505, is shown below the spectrum of IRAS 23060+0505 (Fig. 1*b*). The profile is triangular with FWHM = 1500 km s^{-1}, and represents the observed profile for a filled aperture. Because of guiding errors and seeing fluctuations, I conservatively use 1500 km s^{-1} as the width of the instrumental profile in the analysis that follows.

3. RESULTS

Figure 1 gives the flux calibrated K-band spectra of (*a*) IRAS 20460+1925 and (*b*) IRAS 23060+0505. The error bars represent the internal rms uncertainty for each pixel for the total number of scans used to yield the final spectrum.

The results of the Paα measurements are given in Table 1. The uncertainties in the line fluxes are derived from the formal errors of the continuum least-squares (linear) fit, combined with the uncertainties in the amplitude of the individual pixels of the line profile. Gaussian profiles were fitted to the continuum-subtracted line profiles (Figs. 2*a* and 2*b*) using the general fitting package GAUSSFIT (Jefferys et al. 1988). The quoted uncertainty in FWHM was estimated from that in the least-squares fit combined with the continuum uncertainty. Also quoted in Table 1 are the FWHMs corrected for the estimated instrumental broadening assuming $\mathrm{FWHM}^2_{\mathrm{corr}} = \mathrm{FWHM}^2_{\mathrm{obs}} - \mathrm{FWHM}^2_{\mathrm{inst}}$. The corrected width of Paα in IRAS 23060+0505 is 2900 km s^{-1} compared with its Hα width of 550 km s^{-1}. The corrected width of Paα in IRAS 20460+1925 is 2940 km s^{-1} compared with its Hα width of 2500 km s^{-1}. Therefore both objects contain partially obscured broad line regions (BLRs).

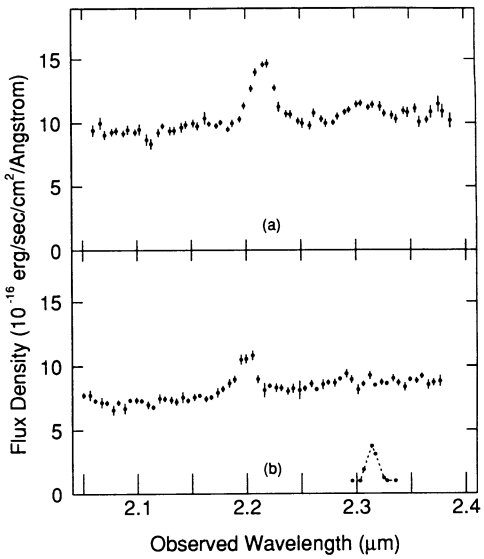

FIG. 1.—(*a*) K-band spectrum of IRAS 20460+1925. Paα is centered at ~2.215 μm and there is a feature at ~2.305 μm that is consistent with Brδ plus a possible contribution from H_2 $S(3)1$–0). (*b*) K-band spectrum of IRAS 23060+0505. Paα is centered at ~2.20 μm and there is also a possible feature at ~2.24 μm that may be due to Brδ. The 1 σ error bars were computed as described in the text. The inset emission line is the unblended 2.314 μm Ar line from the comparison spectrum, which fills the entrance aperture and is sampled as for IRAS 23060+0505. The profile is triangular with width 1500 km s^{-1} (FWHM).

There is an emission feature in the spectrum of IRAS 20460+1925 at an observed wavelength ≈ 2.30 μm. There may be a similar feature in the spectrum of IRAS 23060+0505 at ≈2.29 μm. The central wavelengths of the features are consistent with Brδ. The feature in IRAS 20460+1925 is broad (~3000 km s^{-1}), and there is a hint of asymmetry that may arise from H_2 $S(3)1$–0 emission. Higher resolution and higher sensitivity observations are needed to separate the components.

TABLE 1

PASCHEN-ALPHA MEASUREMENTS

IRAS Name	Line Flux ($\times 10^{14}$) (ergs s^{-1} cm^{-2})	EW[a] (Å)	FWHM (km s^{-1})	FWHM$_{cor}$ (km s^{-1})	FWHM$_{broad}$ (km s^{-1})
20460+1925.....	12.3 ± 0.55	104	3300 ± 160	2940 ± 160	3860[b] ± 300 3420[c] ± 235
23060+0505.....	7.26 ± 0.27	79	3270 ± 270	2900 ± 270	4780 ± 700

[a] Rest frame.
[b] Assumes that the Paα_n width equals the [O III]λ5007 width (FWHM = 1900 km s^{-1}).
[c] Assumes that the Paα_n width equals the Hα width (FWHM = 2500 km s^{-1}).

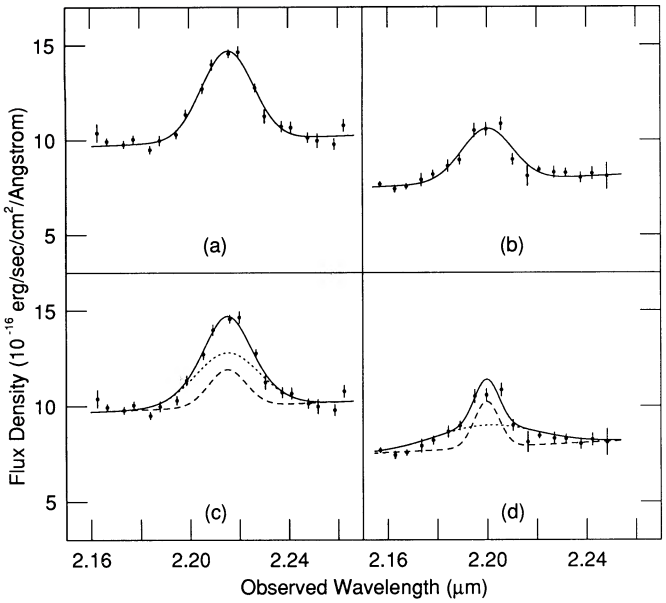

FIG. 2.—Gaussian profile fits to the Paα line profiles for the *K*-band spectra of IRAS 20460+1925 and IRAS 23060+0505: (*a*) a single Gaussian fitted to IRAS 20460+1925, (*b*) a single Gaussian fitted to IRAS 23060+0505, (*c*) the sum (*solid line*) of broad and narrow (*short and long dashes*) Gaussians fitted to IRAS 20460+1925 assuming that the narrow line width is the same as that of [O III]λ5007, (*d*) the sum (*solid line*) of broad and narrow (*short and long dashes*) Gaussians fitted to IRAS 23060+0505 assuming that the narrow line width is the same as that of Hα (see § 4 for details of the fitting procedure).

4. DISCUSSION

4.1. *IRAS 20460+1925*

For IRAS 20460+1925 Frogel et al. (1989) measure a narrow Hα flux $F(\mathrm{H}\alpha)_n = 11.5 \times 10^{-14}$ ergs s^{-1} cm^{-2} and an emission line intensity ratio Hα/Hβ = 6.34 [both corrected for Galactic extinction, $E(B-V) = 0.1$]. Assuming the standard Savage & Mathis (1979) extinction law and Case B recombination implies that $F(\mathrm{Pa}\alpha)_n = 4.4 \times 10^{-14}$ ergs s^{-1} cm^{-2}, leaving $F(\mathrm{Pa}\alpha)_b = 7.9 \times 10^{-14}$ ergs s^{-1} cm^{-2} for the broad component. Different extinction laws (e.g., Howarth 1983; Rieke & Lebofsky 1985) change the derived $F(\mathrm{Pa}\alpha)_n$ by less than 20%. The optical line flux errors dominate the uncertainties in the following analysis.

Since the line widths in Table 1 were determined for the combined narrow and broad Paα components, they underestimate the intrinsic broad line width. The emission-line widths in the NLR are probably well represented by the [O III]λ5007 line width, so I have fitted the Paα profile using a narrow Gaussian having $\mathrm{FWHM}_n = 1900$ km s^{-1} (Frogel et al. 1989) and $\mathrm{F}(\mathrm{Pa}\alpha)_n = 4.4 \times 10^{-14}$ ergs s^{-1} cm^{-2}, plus a Gaussian having width and amplitude as free parameters. The fit was performed using FWHM = 1500 km s^{-1} for the instrumental profile. The best fit gives $\mathrm{FWHM}_b = 3860$ km s^{-1} and $F(\mathrm{Pa}\alpha)_b = 9.1 \times 10^{-14}$ ergs s^{-1} cm^{-2}. Figure 2*c* shows these Gaussian profiles as well as their sum. For completeness, I have repeated the fit (not shown in Fig. 2) using the broader Hα line instead of [O III]. If $\mathrm{FWHM}_n = 2500$ km s^{-1} and $F(\mathrm{Pa}\alpha)_n = 4.4 \times 10^{-14}$ ergs s^{-1} cm^{-2} then $\mathrm{FWHM}_b = 3260$ km s^{-1} and $F(\mathrm{Pa}\alpha)_b = 7.0 \times 10^{-14}$ ergs s^{-1} cm^{-2}.

I have estimated an upper limit to the flux of the broad component of Hα from the spectrum of Frogel et al. (1989), $F(\mathrm{H}\alpha)_b < 2 \times 10^{-14}$ ergs s^{-1} cm^{-2}. Assuming an intrinsic line intensity ratio Paα/Hα = 0.1 typical for UV excess-selected QSOs (Thompson 1991) and the Savage & Mathis (1979) extinction law, I estimate $A_v > 5$ for the intrinsic extinction to the BLR in IRAS 20460+1925. This is not very sensitive to the choice of the narrow line widths; the derived $F(\mathrm{Pa}\alpha)_b$ using different narrow line widths (1900–2500 km s^{-1}) differ by less than 30%.

Although there are uncertainties in estimating an upper limit to $F(\mathrm{H}\alpha)_b$, even if it is 4 times larger [i.e., $F(\mathrm{H}\alpha)_b \approx F(\mathrm{Pa}\alpha)_b$], $A_v > 3.6$. The estimated broad-line extinction is larger than $A_v = 2.2$ derived for the narrow optical emission lines, and is consistent with a longer path length (compared with that for the narrow lines) through dust associated with the NLR, or dust between the BLR and the NLR. However, if a large portion of the observed broad-line spectrum is contributed by a scattered (polarized) component, then the derived extinction may not represent that along the line of sight to the nucleus.

4.2. *IRAS 23060+0505*

Hough et al. (1991) give $A_v = 3.5 \pm 0.5$ (HWB give 3.4 ± 0.5) and $F(\mathrm{H}\alpha)_n = 3.6 \times 10^{-14}$ ergs s^{-1} cm^{-2} for IRAS 23060+0505. Assuming the Savage & Mathis (1979) extinction law and case B recombination, $F(\mathrm{Pa}\alpha)_n = 3.0 \times 10^{-14}$ ergs s^{-1} cm^{-2} ($\pm \sim 30\%$ depending on the extinction law). I have used the procedure outlined above to fit the Paα profile with a Gaussian having $\mathrm{FWHM}_n = 550$ km s^{-1} and $F(\mathrm{Pa}\alpha)_n = 3.0 \times 10^{-14}$ ergs s^{-1} cm^{-2}, plus a Gaussian having width and amplitude as free parameters. The resulting best fit gives $\mathrm{FWHM}_b = 4780$ km s^{-1} and $F(\mathrm{Pa}\alpha)_b = 4.5 \times 10^{-14}$ ergs s^{-1} cm^{-2}. Although single- and two-component fits are consistent with the present data (Figs. 2*b* and 2*d*), the expected contribution to the total Paα flux from the narrow Paα argues for two components (Fig. 2*d*).

Using $\mathrm{F}(\mathrm{H}\alpha)_n$ to scale the spectrum from HWB (their Fig. 3) and a triangular line profile, I estimate $F(\mathrm{H}\alpha)_b \lesssim 2.0 \times 10^{-14}$ ergs s^{-1} cm^{-2}. This implies $A_v \gtrsim 4.4$ to the BLR which is greater than $A_v = 3.5$ derived for the narrow optical emission lines. As for IRAS 20460+1925 this is consistent with a longer path length through dust associated with the NLR, or dust between the BLR and the NLR, but the unknown contribution by the scattered (polarized) component complicates the interpretation.

4.3. *Unified Active Galactic Nucleus Schemes*

Orientation-dependent unification schemes for AGN have been proposed based on polarimetry and spectrophotometry of Sy 2 nuclei (Miller & Goodrich 1990), and higher luminosity AGN such as the QSOs OI 287 (Goodrich & Miller 1989) and IRAS 13349+2438 (Wills et al. 1991). Antonucci & Miller (1985) (see also Miller & Antonucci 1983) have shown that the "prototype" Sy 2 galaxy NGC 1068 has a broad line spectrum hidden behind a dusty torus, that is revealed by broad permitted emission lines scattered (thus polarized) towards the observer. Miller & Goodrich (1990) have detected polarized, broad permitted lines in four other Sy 2 nuclei indicating that at least some Sy 2 nuclei would be classified as Sy 1 if viewed along a different line of sight. Wills et al. (1991) have deduced a similar model for the reddened, highly polarized QSO IRAS 13349+2438 in which a typical QSO nucleus is only partially obscured by a dusty torus that is tilted with respect to our line of sight. Until recently QSOs were thought to be almost dustless; however, the case of IRAS 13349+2438 shows that the viewing angle may determine the selection and classification of even the most luminous AGN.

It has been suggested that Seyfert nuclei are low-luminosity analogs of QSOs, but examples of "QSO 2's" have not been identified previously. Based on their optical spectra and bolometric luminosities alone, the three most luminous known *IRAS*-selected AGN, IRAS 20460+1925, IRAS 23060+0505, and IRAS 09104+4109 (Kleinmann et al. 1988), represent the missing QSO 2's—objects with QSO–like luminosities and "narrow," optical permitted and forbidden emission lines. The fact that both QSO 2's so far investigated harbor hidden QSO 1 nuclei, provides even stronger support for the orientation-dependent AGN unification schemes.

5. SUMMARY

Broad Paα emission has been detected in the narrow-line, extremely luminous galaxies IRAS 20460+1925 and IRAS 23060+0505. The observed FWHM of Paα in IRAS 20460+1925 is 3300 km s^{-1}, with a possible broader component ~3860 km s^{-1}. The observed FWHM of Paα in IRAS 23060+0505 is 3270 km s^{-1}, with a possible broader component ~4780 km s^{-1}. Therefore, considering also their bolometric luminosities, IRAS 20460+1925 and IRAS 23060+0505 should be classified as QSOs. These results argue that there is a population of obscured QSOs (QSO 2), and that they can be selected by their warm (flat) infrared energy distributions and QSO–like luminosities.

It is a pleasure to thank Keith L. Thompson for his assistance during the September 1 observing run, for the use of his software, and for his many helpful suggestions and discussions. I wish to thank Niall Gaffney for assistance during the September 25 run, and for help with the data reduction software. I also wish to thank Beverley J. Wills for suggesting the infrared observations, and for her guidance and support during this project. Thanks also to Gary Hill for helpful discussions and critical readings of the manuscript. It is a pleasure to thank Stefani Eichhorn for assistance in preparation of the final manuscript. Financial support was provided by the McDonald Observatory and by NSF grant AST-8714932.

REFERENCES

Antonucci, R. R. J., & Miller, J. S. 1985, ApJ, 297, 621
Frogel, J. A., Gillett, F. C., Terndrup, D. M., & Vader, J. P. 1989, ApJ, 343, 672
Goodrich, R. W., & Miller, J. S. 1989, ApJ, 346, L21
Hill, G. J., Wynn-Williams, C. G., & Becklin, E. E. 1987, ApJ, 316, L11 (HWB)
Hough, J. H., Brindle, C., Wills, B. J., Wills, D., & Bailey, J. A. 1991, ApJ, in press
Howarth, I. D. 1983, MNRAS, 203, 301
Jefferys, W. H., Fitzpatrick, M. J., McArthur, B. E. 1988, GaussFit: A System for Least Squares and Robust Estimation USERS MANUAL, (Austin: University of Texas).
Kay, L. E., & Miller, J. S. 1989, BAAS, 21, 1099
Kleinmann, S. G., Hamilton, D., Keel, W. C., Wynn-Williams, C. G., Eales, S. A., Becklin, E. E., & Kuntz, K. D. 1988, ApJ, 328, 161
Lester, D. F., Carr, J., Joy, M., & Gaffney, N. 1990, ApJ, 352, 544
Lester, D. F., Harvey, P. M., & Carr, J. 1988, ApJ, 329, 641
Miller, J. S., & Antonucci, R. R. J. 1983, ApJ, 271, L7
Miller, J. S., & Goodrich, R. W. 1990, ApJ, 355, 456
Rieke, G. H., & Lebofsky, M. J. 1985, ApJ, 288, 618
Savage, B. D., & Mathis, J. S. 1979, ARA&A, 17, 73
Thompson, K. L. 1991, Ph.D. thesis, University of Texas
Wills, B. J., Wills, D., Evans, N. J., Natta, A., Thompson, K. L., Breger, M., & Sitko, M. L. 1991, ApJ, submitted